NANO LETTERS

pubs.acs.org/NanoLett Letter

All-Graphene-Contact Electrically Pumped On-Demand Transferrable Nanowire Source

Min-Woo Kim,† Sun-Wook Park,† Kyong-Tae Park,† Byung-Ju Min,† Ja-Hyun Ku, Jin-Yong Ko, Jin Sik Choi, and You-Shin No*

Cite This: *Nano Lett.* 2022, 22, 1316−1323 Read Online

ACCESS | Metrics & More | Article Recommendations | Supporting Information

ABSTRACT: On-demand NW light sources in a photonic integrated circuit (PIC) have faced several practical challenges. Here, we report on an all-graphene-contact, electrically pumped, on-demand transferrable NW source that is fabricated by implementing an all-graphene-contact approach in combination with a highly accurate microtransfer printing technique. A vertically p−i−n-doped top-down-fabricated semiconductor NW with optical gain structures is electrically pumped through the patterned multilayered graphene contacts. Electroluminescence (EL) spectroscopy results reveal that the electrically driven NW device exhibits strong EL emission between the contacts and displays waveguiding properties. Further, a single NW device is precisely integrated into an existing photonic waveguide to perform light coupling and waveguiding experiments. Three-dimensional numerical simulation results show a good agreement with experimental observations. We believe that our all-graphene-contact approach is readily applicable to various micro/nanostructures and devices, which facilitates stable electrical operation and thus extends their practical applicability in compact integrated circuits.

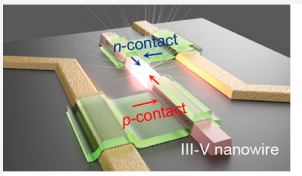

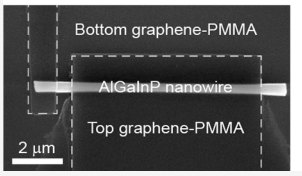

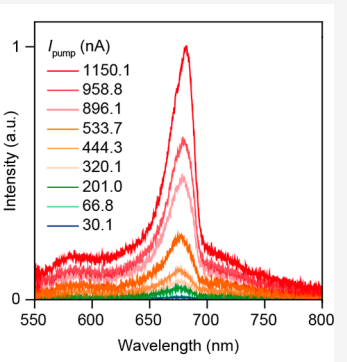

KEYWORDS: *semiconductor nanowires, electrical pumping, on-demand light sources, graphene contacts, numerical simulation, integrated photonic circuits*

Downloaded via KONKUK UNIV on March 2, 2022 at 06:31:10 (UTC).
See https://pubs.acs.org/sharingguidelines for options on how to legitimately share published articles.

INTRODUCTION

Semiconductor nanowires (NWs) are a remarkably versatile class of nanomaterial that have enabled the development of a wide range of devices for nanoelectronics,[1−3] nanobiotechnology,[4−6] photovoltaics,[7−14] nano-optics,[15−30] and quantum photonics.[31−33] In particular, because high-index semiconductor NWs have demonstrated the ability to strongly interact with optical fields and to support distinct resonant modes in nanoscale dimensions, they have been widely applied for the exploration of strong light−matter interactions and to enable enhanced optical functions in diverse systems.[10−18] Such optical properties, which are consistent with essential requirements for high-quality optical cavities, have motivated researchers to consider semiconductor NWs as the most practicable option for efficient light sources in compact photonic integrated circuits (PICs). The III−V or II−VI semiconductor NWs with synthetically controlled electronic band structures have enabled rich spontaneous emission with high quantum efficiency[19−22] and thus been confirmed as high-quality nanoscale light sources that are capable of generating a sufficient amount of light and coupling with other photonic elements.[23−27] However, the direct application of the NW light sources to various PICs have encountered several practical challenges. First, it has been difficult to deterministically register single NWs at target locations with high precision and alignment accuracy. Numerous studies that exploit a variety of forces and techniques (e.g., mechanical,[34] and electrical forces,[35] liquid surface tension,[36,37] and deterministic nano-combing techniques[38]) have been primarily designed to realize the scalable, large-area assembly of NWs in a highly aligned manner. However, the key requirement of PICs is the precise integration of the single NW light sources into the pre-existing passive optical components (e.g., optical waveguides (WG) and modulators). This requirement inevitably necessitates individually addressable/manipulable on-demand registration with nanoscale alignment accuracy,[38−40] which limits the previous efforts to be utilized. Second, it has been considerably difficult to develop a readily applicable and stable scheme for electrical pumping that does not result in significant optical loss. Because the electrical operation of complete photonic circuits, including light sources and other passive optical

Received: November 30, 2021
Revised: January 13, 2022
Published: January 20, 2022

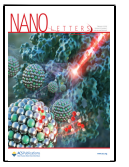

ACS Publications © 2022 American Chemical Society

https://doi.org/10.1021/acs.nanolett.1c04622
Nano Lett. 2022, 22, 1316−1323

elements, is clearly essential for practical purposes, researchers have explored several approaches that entail the use of heavily doped Si substrates and/or conventional metal contacts; they consequently successfully demonstrated the functionality of electrically driven NW light sources.[23,24,27−29] However, the direct contact of Si or metals on a large portion of the light-emitting body causes light to be absorbed over a broad range of optical frequencies, as well as degrades the emission efficiency and subsequent device performance. In addition, the metal contacts that cover a significant portion of the NW typically increase the carrier recombination and help to achieve large spontaneous emission; however, they also block the light that is emitted from the NW, thus preventing the direct coupling of the emitted light to other optical components. Furthermore, the vapor-deposited metals on topologically structured objects sometimes display various sizes of cracks and disconnections owing to the size difference between the objects.[24] Thus, the deposited metals should be thick enough to completely cover the differently sized structures; this consequently further increases the difficulty of integration and the subsequent device fabrication.

In this paper, we report on an all-graphene-contact, electrically pumped, on-demand transferrable NW source. Specifically, we fabricated an all-graphene-contact device by introducing mechanically flexible and optically transparent graphene contacts at the top and bottom surfaces of a semiconductor NW. The vertically p−i−n-doped top-down-fabricated NWs are precisely align-transferred on a target site in a chip by using a microstructured polymer-assisted transfer-printing technique.[39−45] Electroluminescence (EL) spectroscopy was carried out to demonstrate the successful operation of the device and characterize its optical properties. We also coupled an electrically pumped NW source to a strip-type photonic waveguide (SPWG) to demonstrate the on-demand integration and successfully showed light coupling and waveguiding. These observations were quantitatively supported and characterized via numerical simulation.

RESULTS AND DISCUSSION

Figure 1a shows our all-graphene-contact, electrically driven NW light-emitting device. The III−V semiconductor NW, which has a trapezoidal cross section, is electrically p- and n-doped at the top and bottom layers and includes an optical gain medium. The two ultrathin and mechanically flexible graphene patches conformally cover individual metal electrodes and independently connect them to the p-doped top and n-doped bottom surfaces of the NW to serve as the p-contact and n-contact, respectively. These graphene contacts enable the direct injection of carriers into the NW (blue and red arrows in the Figure 1a) and the subsequent radiative recombination. Figure 1b,c shows the low- and high-magnification scanning electron microscopy (SEM) images of a fully fabricated single NW device on a Si_3N_4 substrate. The single AlGaInP NW was separately top-down-fabricated and precisely align-transferred onto a target site on the substrate. Regarding the graphene contacts, we preferentially used chemically synthesized conductive multilayered graphene (MLG) to form a flexible/robust and electrically stable current pathway.[30,46] The bottom and top graphene contacts were lithographically patterned before and after the NW transfer (white dotted lines), which led to the successful realization of a vertically complex top-graphene/NW/bottom-graphene nano-architecture. Under such configuration conditions, the instantaneous physical contact established between the graphene and the surface of the NW enables the formation of an electrical interface that consequently permits current injection.

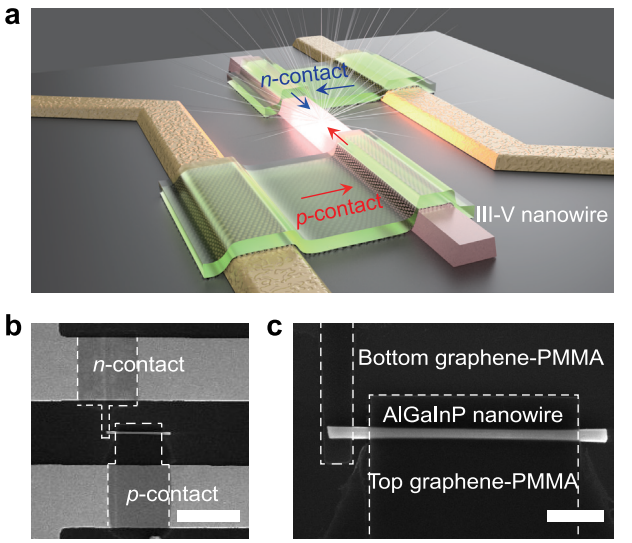

Figure 1. All-graphene-contact, electrically pumped, on-demand transferrable NW light source. (a) Schematic of the device. A single III−V NW is connected to metal electrodes via top (p-contact) and bottom (n-contact) graphene contacts, which are protected by transparent polymer covers (green). Injected carriers (red and blue arrows) are radiatively recombined at the region between the two contacts. (b) Low-magnification SEM image of a fully fabricated single NW device on a Si_3N_4 substrate. The top-down fabricated and vertically p−i−n-doped AlGaInP NW was on-demand registered between two metal electrodes. MLG was used for transparent p- and n-contacts (white dotted lines). Scale bar: 10 μm. (c) High-magnification SEM image of the device. The cross-linked PMMA-patterned top (bottom) graphene layer established direct contact with the top (bottom) layer of the NW. Scale bar: 2 μm.

Our on-chip transferrable all-graphene-contact NW device was fabricated by applying the following processes (Figure 2a−e and Figures S1, S2, Methods in Supporting Information). A commercially available AlGaInP-slab/GaAs-substrate LED wafer was selected for use in the device (Figure S1a). We have applied electron-beam lithography (EBL), chemically assisted dry etching, selective wet etching, and oxygen plasma cleaning processes to fabricate an array of nanoscale wires and two separate mesa structures (Figure 2a and Figure S1b, Methods). Following fabrication, the NWs with both ends connected to mesa structures were kept air-suspended (Figure 2a). Evidently, the air spacing underneath the NWs in the presence of the bulk-supporting mesa structures can facilitate the pick-up and separation process during transfer printing.

In addition, we employed a focused ion beam to section the fabricated NWs in a direction perpendicular to the NW axis. The high-magnification transmission electron microscopy (TEM) image in Figure 2c reveals the cross-sectional geometry and compositional structure of a NW. Regarding the cross section, a slight sidewall slope arising from the mechanical etching process led to the formation of the trapezoidal cross-sectional shape.[47] Therefore, one can readily identify the cross-sectional orientation based on the shape and determine the electrical polarity of the NW as well. In addition, the sidewall slope provides a better topological condition when the top

https://doi.org/10.1021/acs.nanolett.1c04622
Nano Lett. 2022, 22, 1316−1323

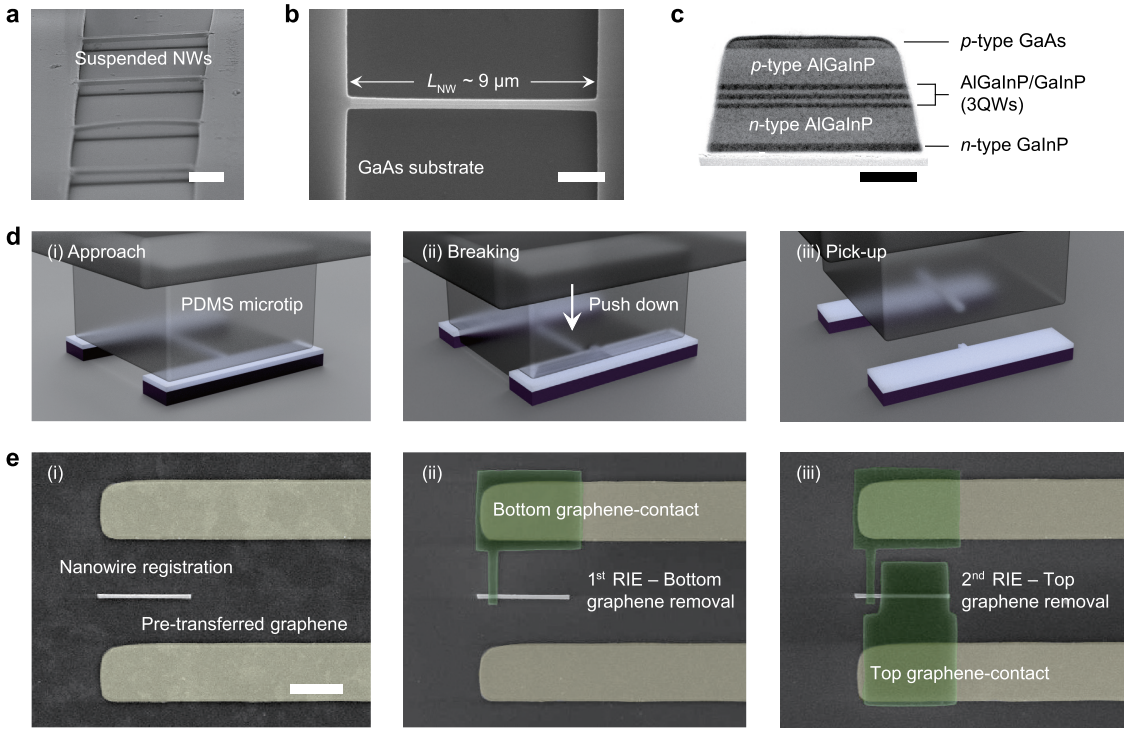

Figure 2. Fabrication process for an on-demand transferrable all-graphene-contact NW device. (a) Tilted-view SEM image of the top-down-fabricated AlGaInP NW array. Scale bar: 2 μm. (b) Top-view SEM image of a single NW; length, ~9 μm; width, ~300 nm; thickness, 200 nm. Scale bar: 2 μm. NW ends were connected to the supporting mesa structures, and the entire body of the NW was air-suspended. (c) Cross-sectional TEM image of a single NW showing vertically p-type/intrinsic/n-type doped layers and MQW structures. Scale bar: 100 nm. (d) Schematics showing how the PDMS microtip is employed for pick up: (i) the microtip approach, (ii) breaking of the NW terminals, and (iii) the pick-up. (e) Top-view false-colored SEM images showing the key fabrication steps for the on-demand all-graphene-contact device: (i) align-registration of a NW on a device site posterior to transferring the bottom graphene layer (scale bar: 5 μm), (ii) definition of the bottom graphene contact via lithographic patterning and dry etching, and (iii) definition of the top graphene contact by repeating (i) and (ii).

graphene contact is conformally applied to the top surface of the NW.

Next, we individually addressed and picked up the fabricated NWs by using the previously developed transfer-printing setup.[39] Figure 2d schematically illustrates this process, which can be described as follows. The microscale cubical polydimethylsiloxane (PDMS) tip is aligned with respect to the boundary lines of the mesa structures and approached to a single NW (Figure 2d (i)). A gentle downward force is applied after contact is established and both terminals of the NW are easily broken, resulting in separation from the supporting mesa structure (Figure 2d (ii)). Then, a simple upward translation of the PDMS microtip terminates the pick-up process (Figure 2d (iii)). Although this process worked well with the most wire-typed nanostructures, it was sometimes limited to picking up the structures that were shorter than ~7 μm and/or wider than ~500 nm. For those structures, we have developed a unique two-step pick-up and transfer process (Figure S2) that takes full advantage of the optical and mechanical properties of PDMS microtips, for example, high optical transparency in the visible wavelengths, good mechanical flexibility, and controllable adhesive force.[39−45] We believe that the above-described two-step transfer technique is simple and readily applicable to a variety of micro/nanostructures and thus useful for many applications that require highly accurate hybrid and/or heterogeneous on-chip integration.

In parallel, we developed the fabrication procedure for an all-graphene-contact device (Figure 2e). First, we used a conventional wet-transfer technique[48] to separate a sheet of chemical vapor deposition (CVD)-grown MLG from its growth substrate and enable its transfer to a metallized Si_3N_4 substrate (see Methods). Regarding the MLG, the results of topographical, optical, and electrical measurements, respectively, confirmed high uniformity in thickness, high optical transmission in the visible wavelength range,[49] and good electrical conduction,[50] which are essential properties for electrical contact of light-emitting devices (Figure S3). Then, we exploited the characteristics of the PDMS microtip to precisely align-register the individual NWs on top of the graphene (Figure 2e (i)). Next, we utilized the cross-linked polymer resist to lithographically pattern the bottom graphene contact and removed the nonpatterned areas of graphene via a reactive ion-etching (RIE) process (Figure 2e (ii)). Lastly, we repeated the steps given as Figure 2e(i) and (ii) to define the top graphene contact to complete the fabrication process (Figure 2e (iii)). We note that our all-graphene-contact approach is a unique and advantageous approach that circumvents various problems and difficulties that are commonly associated with the conventional method, such as those related to the requirement for the nanoscale structures or materials with vertical doping to be heterogeneously integrated and electrically operated. In particular, the definition of the metallic contacts on the top and bottom of a nanoscale structure requires individually controllable nanoscale manipulation of the target object; the structure must be metallized on one surface, and then completely turned upside down and repositioned at the same location for the second metallization on the opposite surface. As can be expected, these processes

https://doi.org/10.1021/acs.nanolett.1c04622
Nano Lett. 2022, 22, 1316−1323

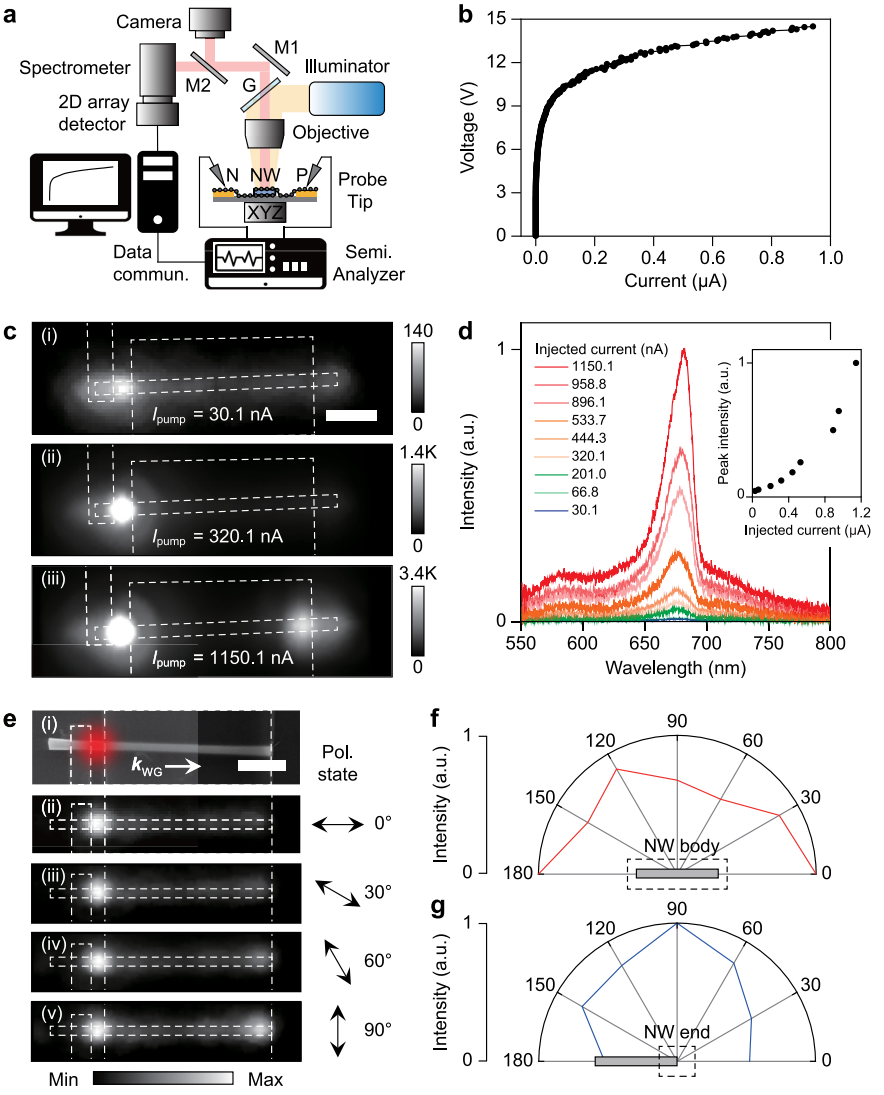

Figure 3. Spectroscopic characterizations. (a) EL imaging and spectroscopy setup. A semiconductor parameter analyzer was used to inject CW currents into the device as emitted EL was either imaged on CCD or sent to a spectrometer. (b) Measured $I-V$ curve for the NW device shown in Figure 1c. (c) CCD-generated EL emission patterns obtained at different levels of injected current: (i) low current (I_{pump} = 30.1 nA), (ii) moderate current (I_{pump} = 320.1 nA), and (iii) high current (I_{pump} = 1150.1 nA). Each CCD-generated image was normalized according to the maximum intensity. The white dotted lines mark the graphene contacts and NW. Scale bar: 2 μm. (d) EL spectra measured under the conditions of injected current ranging from 30.1 to 1150.1 nA; inset: the maximum intensity plotted as a function of injected current. (e) Angle-resolved EL imaging results obtained by using a linear polarizer. (i) SEM images of the NW device used in the experiment. Scale bar: 2 μm. (ii)−(v) EL emission patterns (left) associated with different transmission axes (black arrows, right). The angles between the NW and transmission axes were as follows: (ii) 0°, (iii) 30°, (iv) 60°, and (v) 90°. (f,g) Angle-resolved EL intensity distributions. The EL intensities were collected for a small window that included the (f) entire body of the NW and (g) one end of the NW near the boundaries of the graphene contact. The intensities shown in each plot were normalized according to its maximum.

are extremely complex and limited unless one has access to the cutting-edge technology for this special purpose.[51,52] In addition, these top and bottom contacts must be extended and connected to the existing larger metal electrodes, which requires additional lithography and metallization. Furthermore, the definition of the metal contacts on top of or near optical/photonic or optoelectronic devices can result in unwanted optical losses, deteriorate the intrinsic optical properties of the materials, and degrade the device performance. However, our all-graphene-contact approach does not require nanoscale manipulation, multiple rounds of metallization or additional extension to outer electrodes. In addition, the graphene is optically transparent over a broad range of optical and near-infrared frequencies; this results in significantly less optical loss than the metals that are conventionally employed for contact (e.g., Cr, Ti, and Au).

We carried out EL spectroscopy to investigate the optical characteristics of our device. The fully fabricated single NW device shown in Figure 1c was electrically pumped with continuous-wave (CW) currents at room temperature by using two metallic probe tips connected to a semiconductor parameter analyzer (Figure 3a and Methods). The EL emitted by the device was then collected by a ×50 microscope objective lens and either passed to the spectrometer or imaged onto a highly sensitive charge-coupled device (CCD). Before performing the optical measurements, we briefly investigated the electrical transport properties of our device by measuring the current−voltage ($I-V$) curve (Figure 3b). The $I-V$ data

https://doi.org/10.1021/acs.nanolett.1c04622
Nano Lett. 2022, 22, 1316−1323

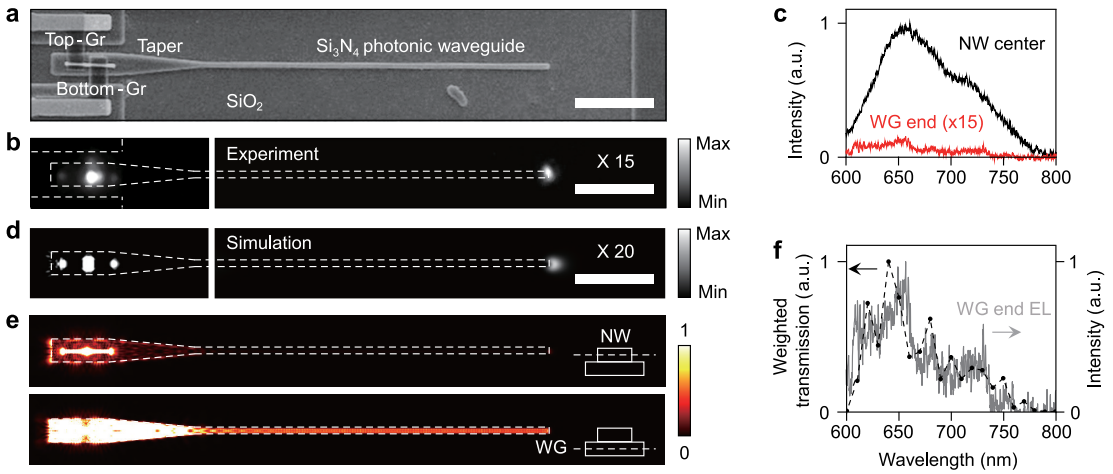

Figure 4. Electrically pumped on-demand NW source. (a) SEM image of an all-graphene-contact NW source with a single Si_3N_4 SPWG. The WG structure includes a NW coupling region (coupling area, A_{NW}, 3 × 10 μm^2), a linearly tapered section (tapering length, L_{taper}, 11 μm), and a single strip WG (strip length, L_{strip}, 50 μm). Scale bar: 10 μm. (b) CCD images of the EL emission from the NW source (left), and the waveguided and scattered EL intensities at the end of the WG (right). Scale bar: 10 μm. (c) EL spectra measured at the NW center (black) and WG end (red). Note that the intensities at the end of the WG in (b,c) were increased 15-fold for comparison. (d) Calculated z-component of the time-averaged Poynting vectors for the NW ($\langle P_z \rangle_{NW}$, left) and end of the WG ($\langle P_z \rangle_{WG}$, right). Dipole sources with a wavelength of 660 nm were generated at the center of the NW. The Poynting vectors were measured at 500 nm above the top surface of the NW. The values of $\langle P_z \rangle_{WG}$ were increased 20-fold for comparison. (e) Field-intensity distributions at the center of the NW (top) and WG (bottom). (f) Calculated weighted transmission plotted as a function of the wavelength of the dipole source. The measured spectral profile of the NW in (c) was considered to be the spectral profile emitted from the dipoles in the simulation to weight the relative spectral power of the source. Note that the contributions of all electric dipoles (i.e., E_x, E_y, E_z) were included in panels d–f.

confirmed typical diode-like characteristics with the onset of current flow at a forward bias of ~8.4 V, which was followed by an exponential increase in the current; specifically, when the applied voltage ranged from 10.0 to 14.0 V, the measured currents significantly increased from 77.4 to 735.4 nA. Although different materials and device structures caused variation among some characteristics (e.g., turn-on voltage and current flow levels), the observed transport behaviors were qualitatively similar to those of previously reported NW devices that utilize graphene contacts.[30] Overall, these results confirm the successful formation of a current path, as well as the necessary electrical operations.

To characterize the light-emitting properties, we systematically varied the amount of injected current, (i.e., I_{pump}) and subsequently observed the pattern of EL emission from the device and measured the spectrum (Figure 3c,d). Regarding the results, we observed strong light emission between the p-type bottom graphene contact and n-type top graphene contact at all current levels; conversely, relatively weak emission from the entire body of the NW was only observed at low current levels (Figure 3c (i)). As we gradually increased I_{pump}, the EL intensity between the two contacts was significantly enhanced, whereas only a small change in intensity was observed from the NW body (Figure 3c (ii)). These observations revealed that the recombination primarily takes place in a way that satisfies the least path for charge carriers to transport. These results were also consistent with those previously obtained for single NW LEDs that employed conventional metal contacts.[24] In addition, numerical simulation results show that our graphene contacts absorbed much less light compared to conventional metal contacts (Figure S5). Therefore, we concluded that our graphene contact functions properly as an electrical contact. More interestingly, as we further increased I_{pump}, pronounced EL intensities other than the aforementioned strong emission were observed in the region wherein the NW body met the boundaries of the top graphene contact (Figure 3c (iii)). The measured intensities were not as high as those of the strong one, but they were stronger than those from the other regions of the NW body. This behavior was consistently found in multiple devices, suggesting that it was unlikely to be attributable to the irregular properties of certain devices. We believe that this emergence of local EL intensities is primarily because of the light scattering of propagating WG modes of the NW.[19] We will expound upon this in a later discussion on a set of supporting experiments and the corresponding data analysis (Figure 3e–g). The measured EL spectra presented in Figure 3d show the AlGaInP MQW emission centered at ~680 nm; this figure also clearly shows the development of spectral light intensity as a function of the injected current. Here, we obtained all of the EL spectra by collecting light from a small window that only includes the strong emission that was measured between the two graphene contacts.

We further characterized the light-emitting properties by performing angle-resolved imaging and spectroscopy (Figure 3e–g). Figure 3e shows an SEM image of the single NW device (Figure 3e (i)) and a series of EL images that were captured under the conditions of different transmission axes (Figure 3e (ii)–(v)). The NW device was electrically pumped at a sufficiently high level of current (i.e., 4492.6 nA) to ensure that the local EL intensity appears near the boundaries of the graphene contact. As was expected, the strong emission between the two graphene contacts remained nearly unchanged for all transmission axes because of the unpolarized nature of the spontaneous emission. However, the local EL intensity signals disappeared when the transmission axis was parallel to the axis of the NW (Figure 3e (ii)). As we changed the transmission axis, gradually shifting it to become perpendicular to the NW axis, the intensity signals increased (Figure 3e (iii),(iv)), becoming maximized at a right angle (Figure 3e (v)). These observations were also supported by

https://doi.org/10.1021/acs.nanolett.1c04622
Nano Lett. 2022, 22, 1316–1323

the intensity angle distribution results shown in Figure 3f,g; specifically, unlike the results for the light emitted from the NW body, the results for the angle distribution of intensities measured at one end of the NW clearly indicated linearly polarized characteristics. The results of these angle-resolved experiments revealed that no additional current channel or subsequent radiative recombination contributed to the local EL intensities. Instead, taking into consideration the transverse wave nature of light, the results suggest that the intensity signals likely originated from the propagating light that had wavevectors aligned to the NW axis ($\mathbf{k}_{WG}$ in Figure 3e (i)). For example, under the conditions of strong light emission between the two graphene contacts, a portion of the light is coupled to the propagating WG modes of the NW. Then, the light scatters upon experiencing an abrupt change in the index of environment; in the case of our design, the few-hundred-nanometer-thick protective polymer that covers the graphene contact defines the boundaries. This results in the scattered light intensities being locally observed near the boundaries. Thus, we have successfully demonstrated the electrically pumped light emission from an on-chip, transferrable, all-graphene-contact nanodevice, and revealed the waveguiding characteristics of the emitted light.

The results shown in Figure 3 strongly encouraged us to realize an on-demand electrically pumped nanoscale light source in a PIC. As a simple proof-of-concept demonstration, we first fabricated an array of single SPWGs on a Si_3N_4 device chip (Figure S6, Methods). Then we heterogeneously integrated a single NW device with these SPWGs and carried out a light coupling and waveguiding experiment (Figure 4). Figure S6c shows a representative SEM image of a 70 μm long Si_3N_4 SPWG with three distinctive regions: a 3 μm wide coupling region for a NW light source (I), a linearly tapered section for efficient light coupling (II),[52] and a single strip for waveguiding (III). The single NWs were align-transferred at the center of the coupling region of the SPWGs (Figure 4a). Regarding the transfer-printing process, the vertical and rotational misalignments were typically less than 100 nm and 1.0°, respectively, thus confirming highly accurate integration with nanoscale alignment and precision (Figure S7).

To perform the optical experiment, we applied I_{pump} = 825.7 nA to electrically pump the NW; we then recorded the EL intensities at the NW center (left, Figure 4b) and SPWG end (right, Figure 4b). The EL intensities measured at the end of the WG confirm that a portion of the EL emitted from the NW device was successfully coupled to the guided modes, propagated through the SPWG, and scattered at the WG termination point. The measured spectra shown in Figure 4c further demonstrate the spectral ratios of the z-component of the EL intensities measured between the two locations; specifically, the maximum intensity ratio of $I_{z,WG}/I_{z,NW}$ was estimated to be ~1.0% at a wavelength of 660 nm, which is comparable to the ratios obtained in previous studies that employed NW and WG integrated structures.[23,24]

To obtain an in-depth understanding of coupling and waveguiding, we performed three-dimensional finite-difference time-domain (FDTD) simulations (Figures S8−10, Methods). We first investigated the modal properties of the single strip WG (Figure S8), and then simulated the light coupling and waveguiding characteristics of the integrated structure used in the experiment (Figure S9a) by introducing electric dipoles (i.e., E_x, E_y, and E_z) at the center of the NW (Figure S9b−d). Figure 4d shows the calculated z-component of the time-averaged Poynting vectors, $\langle P_z \rangle$ (top panels of Figure S9b−d). The simulated results were clearly a reproduction of what was observed during the experiment; thus, the results confirmed the extent of the contribution of the polarized light that was emitted from the NW to the propagated and scattered light at the end of the SPWG. The top and bottom panels of Figure 4e, respectively, show the field-intensity distributions at the center of the NW and WG; this figure also illustrates how the electric fields were coupled and propagated through the SPWG. We also calculated the dipole powers (P_{dipole}) of the generated dipoles and transmitted powers (P_{trans}) passing through the SPWG and quantified the transmission as the ratio of P_{trans}/P_{dipole} (Figure S9e, Methods).[24,40] We utilized the data for all three polarizations, as well as the experimentally measured spectral profile of the NW, to estimate the weighted transmission as a function of wavelength (Figure 4f). To enable direct comparison, the experimentally measured spectrum corresponding to the end of the WG (red, Figure 4c) is also included in the graph. Surprisingly, the numerically estimated data was in excellent agreement with the measurement results; particularly, the trends of the weighted transmissions were well-represented in the experimentally measured structured spectrum. Thus, we believe that the results and analysis presented in Figure 4 confirm the direct and successful demonstration of our electrically pumped, on-demand nanoscale source in a chip.

CONCLUSIONS

In summary, we have demonstrated the functionality of an on-demand transferrable, electrically pumped NW light source by implementing a unique all-graphene-contact approach. Top-down-fabricated AlGaInP NWs with vertical p−i−n doping were precisely align-transferred on a target site by using the microtip-assisted transfer-printing technique, and electrically operated through the use of top and bottom graphene contacts. The results of spectroscopic measurement allowed us to investigate the emission characteristics of our device by analyzing the strong EL signal that was emitted from the NW and waveguided EL intensities at the end of the NW. We integrated a prefabricated SPWG into our device and confirmed successful light coupling and waveguiding. Numerical simulations were also performed to reproduce the experimental observations and allow detailed analysis of the light coupling and transmission. Our all-graphene-contact approach may potentially be applied to a variety of nanomaterials and nanostructures, as well as nano/microscale optical devices,[10−13,19,24,28,29,53−60] and easily exploited to realize more complex nanoarchitectures in an integrated optical circuit.

ASSOCIATED CONTENT

Supporting Information

The Supporting Information is available free of charge at https://pubs.acs.org/doi/10.1021/acs.nanolett.1c04622.

Methods and figures; Figure S1, structure of wafer and NWs fabrication; Figure S2, two-step pick-up and transfer process; Figure S3, characterization of MLG; Figure S4, cross-sectional TEM image; Figure S5, relative light absorption; Figure S6, fabrication process for an array of SPWGs; Figure S7, misalignment measurement; Figure S8, dispersions and field profiles of SPWG; Figure S9, numerical simulation in the SPWG

https://doi.org/10.1021/acs.nanolett.1c04622
Nano Lett. 2022, 22, 1316−1323

coupled to a NW; Figure S10, calculated transmission results (PDF)

AUTHOR INFORMATION

Corresponding Author

You-Shin No − *Department of Physics, Konkuk University, Seoul 05029, Republic of Korea;* orcid.org/0000-0001-8947-4189; Phone: +82-2-450 3419; Email: ysno@konkuk.ac.kr

Authors

Min-Woo Kim − *Department of Physics, Konkuk University, Seoul 05029, Republic of Korea*

Sun-Wook Park − *Department of Physics, Konkuk University, Seoul 05029, Republic of Korea*

Kyong-Tae Park − *Department of Physics, Konkuk University, Seoul 05029, Republic of Korea*

Byung-Ju Min − *Department of Physics, Konkuk University, Seoul 05029, Republic of Korea*

Ja-Hyun Ku − *Department of Physics, Konkuk University, Seoul 05029, Republic of Korea*

Jin-Yong Ko − *Department of Physics, Konkuk University, Seoul 05029, Republic of Korea*

Jin Sik Choi − *Department of Physics, Konkuk University, Seoul 05029, Republic of Korea*

Complete contact information is available at: https://pubs.acs.org/10.1021/acs.nanolett.1c04622

Author Contributions

†M.-W.K., S.-W.P., K.-T.P., and B.-J.M. have contributed equally to this work.

Notes

The authors declare no competing financial interest.

ACKNOWLEDGMENTS

Y.-S.N. acknowledges the support from the National Research Foundation of Korea (NRF) grant funded by the Korean government (2018R1C1B3001130).

REFERENCES

(1) Tian, B.; Zheng, X.; Kempa, T. J.; Fang, Y.; Yu, N.; Yu, G.; Huang, J.; Lieber, C. M. Coaxial silicon nanowires as solar cells and nanoelectronic power sources. *Nature* **2007**, *449* (7164), 885−889.

(2) Yan, H.; Choe, H. S.; Nam, S.; Hu, Y.; Das, S.; Klemic, J. F.; Ellenbogen, J. C.; Lieber, C. M. Programmable nanowire circuits for nanoprocessors. *Nature* **2011**, *470* (7333), 240−244.

(3) Yao, J.; Yan, H.; Das, S.; Klemic, J. F.; Ellenbogen, J. C.; Lieber, C. M. Nanowire nanocomputer as a finite-state machine. *Proc. Natl. Acad. Sci. U. S. A.* **2014**, *111* (7), 2431−2435.

(4) Tian, B.; Cohen-Karni, T.; Qing, Q.; Duan, X.; Xie, P.; Lieber, C. M. Three-Dimensional, Flexible Nanoscale Field-Effect Transistors as Localized Bioprobes. *Science* **2010**, *329* (5993), 830−834.

(5) Qing, Q.; Jiang, Z.; Xu, L.; Gao, R.; Mai, L.; Lieber, C. M. Free-standing kinked nanowire transistor probes for targeted intracellular recording in three dimensions. *Nat. Nanotechnol.* **2014**, *9* (2), 142−147.

(6) Zhou, W.; Dai, X.; Lieber, C. M. Advances in nanowire bioelectronics. *Rep. Prog. Phys.* **2017**, *80* (1), 016701.

(7) Espinet-Gonzalez, P.; Barrigón, E.; Otnes, G.; Vescovi, G.; Mann, C.; France, R. M.; Welch, A. J.; Hunt, M. S.; Walker, D.; Kelzenberg, M. D.; Åberg, I.; Borgström, M. T.; Samuelson, L.; Atwater, H. A. Radiation Tolerant Nanowire Array Solar Cells. *ACS Nano* **2019**, *13* (11), 12860−12869.

(8) Fountaine, K. T.; Cheng, W.-H.; Bukowsky, C. R.; Atwater, H. A. Near-Unity Unselective Absorption in Sparse InP Nanowire Arrays. *ACS Photonics* **2016**, *3* (10), 1826−1832.

(9) Gu, Y.; Kwak, E.-S.; Lensch, J. L.; Allen, J. E.; Odom, T. W.; Lauhon, L. J. Near-field scanning photocurrent microscopy of a nanowire photodetector. *Appl. Phys. Lett.* **2005**, *87* (4), 043111.

(10) Cao, L.; White, J. S.; Park, J.-S.; Schuller, J. A.; Clemens, B. M.; Brongersma, M. L. Engineering light absorption in semiconductor nanowire devices. *Nat. Mater.* **2009**, *8* (8), 643−647.

(11) Kim, S.-K.; Day, R. W.; Cahoon, J. F.; Kempa, T. J.; Song, K.-D.; Park, H.-G.; Lieber, C. M. Tuning Light Absorption in Core/Shell Silicon Nanowire Photovoltaic Devices through Morphological Design. *Nano Lett.* **2012**, *12* (9), 4971−4976.

(12) Kempa, T. J.; Cahoon, J. F.; Kim, S.-K.; Day, R. W.; Bell, D. C.; Park, H.-G.; Lieber, C. M. Coaxial multishell nanowires with high-quality electronic interfaces and tunable optical cavities for ultrathin photovoltaics. *Proc. Natl. Acad. Sci. U. S. A.* **2012**, *109* (5), 1407−1412.

(13) Fan, P.; Yu, Z.; Fan, S.; Brongersma, M. L. Optical Fano resonance of an individual semiconductor nanostructure. *Nat. Mater.* **2014**, *13* (5), 471−475.

(14) Brongersma, M. L.; Cui, Y.; Fan, S. Light management for photovoltaics using high-index nanostructures. *Nat. Mater.* **2014**, *13* (5), 451−460.

(15) Miyata, M.; Holsteen, A.; Nagasaki, Y.; Brongersma, M. L.; Takahara, J. Gap Plasmon Resonance in a Suspended Plasmonic Nanowire Coupled to a Metallic Substrate. *Nano Lett.* **2015**, *15* (8), 5609−5616.

(16) Kim, S.; Kim, K.-H.; Hill, D. J.; Park, H.-G.; Cahoon, J. F. Mie-coupled bound guided states in nanowire geometric superlattices. *Nat. Commun.* **2018**, *9* (1), 2781.

(17) Kim, S.; Kim, K.-H.; Cahoon, J. F. Optical Bound States in the Continuum with Nanowire Geometric Superlattices. *Phys. Rev. Lett.* **2019**, *122* (18), 187402.

(18) Gloppe, A.; Verlot, P.; Dupont-Ferrier, E.; Siria, A.; Poncharal, P.; Bachelier, G.; Vincent, P.; Arcizet, O. Bidimensional nano-optomechanics and topological backaction in a non-conservative radiation force field. *Nat. Nanotechnol.* **2014**, *9* (11), 920−926.

(19) Qian, F.; Gradečak, S.; Li, Y.; Wen, C.-Y.; Lieber, C. M. Core/Multishell Nanowire Heterostructures as Multicolor, High-Efficiency Light-Emitting Diodes. *Nano Lett.* **2005**, *5* (11), 2287−2291.

(20) Gargas, D. J.; Gao, H.; Wang, H.; Yang, P. High Quantum Efficiency of Band-Edge Emission from ZnO Nanowires. *Nano Lett.* **2011**, *11* (9), 3792−3796.

(21) Agarwal, R.; Barrelet, C. J.; Lieber, C. M. Lasing in Single Cadmium Sulfide Nanowire Optical Cavities. *Nano Lett.* **2005**, *5* (5), 917−920.

(22) Qian, F.; Li, Y.; Gradečak, S.; Park, H.-G.; Dong, Y.; Ding, Y.; Wang, Z. L.; Lieber, C. M. Multi-quantum-well nanowire heterostructures for wavelength-controlled lasers. *Nat. Mater.* **2008**, *7* (9), 701−706.

(23) Park, H.-G.; Barrelet, C. J.; Wu, Y.; Tian, B.; Qian, F.; Lieber, C. M. A wavelength-selective photonic-crystal waveguide coupled to a nanowire light source. *Nat. Photonics* **2008**, *2* (10), 622−626.

(24) No, Y.-S.; Choi, J.-H.; Ee, H.-S.; Hwang, M.-S.; Jeong, K.-Y.; Lee, E.-K.; Seo, M.-K.; Kwon, S.-H.; Park, H.-G. A Double-Strip Plasmonic Waveguide Coupled to an Electrically Driven Nanowire LED. *Nano Lett.* **2013**, *13* (2), 772−776.

(25) Takiguchi, M.; Takemura, N.; Tateno, K.; Nozaki, K.; Sasaki, S.; Sergent, S.; Kuramochi, E.; Wasawo, T.; Yokoo, A.; Shinya, A.; Notomi, M. All-Optical InAsP/InP Nanowire Switches Integrated in a Si Photonic Crystal. *ACS Photonics* **2020**, *7* (4), 1016−1021.

(26) Birowosuto, M. D.; Yokoo, A.; Zhang, G.; Tateno, K.; Kuramochi, E.; Taniyama, H.; Takiguchi, M.; Notomi, M. Movable high-Q nanoresonators realized by semiconductor nanowires on a Si photonic crystal platform. *Nat. Mater.* **2014**, *13* (3), 279−285.

(27) Fan, P.; Colombo, C.; Huang, K. C. Y.; Krogstrup, P.; Nygård, J.; Fontcuberta I Morral, A.; Brongersma, M. L. An Electrically-Driven

GaAs Nanowire Surface Plasmon Source. *Nano Lett.* **2012**, *12* (9), 4943−4947.
(28) Duan, X.; Huang, Y.; Agarwal, R.; Lieber, C. M. Single-nanowire electrically driven lasers. *Nature* **2003**, *421* (6920), 241−245.
(29) Bao, J.; Zimmler, M. A.; Capasso, F.; Wang, X.; Ren, Z. F. Broadband ZnO Single-Nanowire Light-Emitting Diode. *Nano Lett.* **2006**, *6* (8), 1719−1722.
(30) Tchernycheva, M.; Lavenus, P.; Zhang, H.; Babichev, A. V.; Jacopin, G.; Shahmohammadi, M.; Julien, F. H.; Ciechonski, R.; Vescovi, G.; Kryliouk, O. InGaN/GaN Core-Shell Single Nanowire Light Emitting Diodes with Graphene-Based P-Contact. *Nano Lett.* **2014**, *14* (5), 2456−2465.
(31) Korzh, B.; Zhao, Q.-Y.; Allmaras, J. P.; Frasca, S.; Autry, T. M.; Bersin, E. A.; Beyer, A. D.; Briggs, R. M.; Bumble, B.; Colangelo, M.; Crouch, G. M.; Dane, A. E.; Gerrits, T.; Lita, A. E.; Marsili, F.; Moody, G.; Peña, C.; Ramirez, E.; Rezac, J. D.; Sinclair, N.; Stevens, M. J.; Velasco, A. E.; Verma, V. B.; Wollman, E. E.; Xie, S.; Zhu, D.; Hale, P. D.; Spiropulu, M.; Silverman, K. L.; Mirin, R. P.; Nam, S. W.; Kozorezov, A. G.; Shaw, M. D.; Berggren, K. K. Demonstration of sub-3 ps temporal resolution with a superconducting nanowire single-photon detector. *Nat. Photonics* **2020**, *14* (4), 250−255.
(32) Yu, Y.; Dou, X.-M.; Wei, B.; Zha, G.-W.; Shang, X.-J.; Wang, L.; Su, D.; Xu, J.-X.; Wang, H.-Y.; Ni, H.-Q.; Sun, B.-Q.; Ji, Y.; Han, X.-D.; Niu, Z.-C. Self-Assembled Quantum Dot Structures in a Hexagonal Nanowire for Quantum Photonics. *Adv. Mater.* **2014**, *26* (17), 2710−2717.
(33) Babinec, T. M.; Hausmann, B. J. M.; Khan, M.; Zhang, Y.; Maze, J. R.; Hemmer, P. R.; Lončar, M. A diamond nanowire single-photon source. *Nat. Nanotechnol.* **2010**, *5* (3), 195−199.
(34) Fan, Z.; Ho, J. C.; Jacobson, Z. A.; Yerushalmi, R.; Alley, R. L.; Razavi, H.; Javey, A. Wafer-Scale Assembly of Highly Ordered Semiconductor Nanowire Arrays by Contact Printing. *Nano Lett.* **2008**, *8* (1), 20−25.
(35) Freer, E. M.; Grachev, O.; Duan, X.; Martin, S.; Stumbo, D. P. High-yield self-limiting single-nanowire assembly with dielectrophoresis. *Nat. Nanotechnol.* **2010**, *5* (7), 525−530.
(36) Cao, Q.; Han, S.-J.; Tulevski, G. S.; Zhu, Y.; Lu, D. D.; Haensch, W. Arrays of single-walled carbon nanotubes with full surface coverage for high-performance electronics. *Nat. Nanotechnol.* **2013**, *8* (3), 180−186.
(37) Yu, G.; Cao, A.; Lieber, C. M. Large-area blown bubble films of aligned nanowires and carbon nanotubes. *Nat. Nanotechnol.* **2007**, *2* (6), 372−377.
(38) Yao, J.; Yan, H.; Lieber, C. M. A nanoscale combing technique for the large-scale assembly of highly aligned nanowires. *Nat. Nanotechnol.* **2013**, *8* (5), 329−335.
(39) Park, S.-W.; Kim, M.-W.; Park, K.-T.; Ku, J.-H.; No, Y.-S. On-Chip Transferrable Microdisk Lasers. *ACS Photonics* **2020**, *7* (12), 3313−3320.
(40) Lee, J.; Karnadi, I.; Kim, J. T.; Lee, Y.-H.; Kim, M.-K. Printed Nanolaser on Silicon. *ACS Photonics* **2017**, *4* (9), 2117−2123.
(41) Guilhabert, B.; McPhillimy, J.; May, S.; Klitis, C.; Dawson, M. D.; Sorel, M.; Strain, M. J. Hybrid integration of an evanescently coupled AlGaAs microdisk resonator with a silicon waveguide by nanoscale-accuracy transfer printing. *Opt. Lett.* **2018**, *43* (20), 4883−4886.
(42) Kim, Y.; Park, B. J.; Kim, M.; Song, D. I.; Lee, J.; Yu, A.; Kim, M.-K. Hybrid Silicon Microlasers with Gain Patches of Unlimited Designs. *ACS Photonics* **2021**, *8* (9), 2590−2597.
(43) Zhang, J.; Muliuk, G.; Juvert, J.; Kumari, S.; Goyvaerts, J.; Haq, B.; Op de Beeck, C.; Kuyken, B.; Morthier, G.; Van Thourhout, D.; Baets, R.; Lepage, G.; Verheyen, P.; Van Campenhout, J.; Gocalinska, A.; O'Callaghan, J.; Pelucchi, E.; Thomas, K.; Corbett, B.; Trindade, A. J.; Roelkens, G. III-V-on-Si photonic integrated circuits realized using micro-transfer-printing. *APL Photonics* **2019**, *4* (11), 110803.
(44) Perl, A.; Reinhoudt, D. N.; Huskens, J. Microcontact Printing: Limitations and Achievements. *Adv. Mater.* **2009**, *21* (22), 2257−2268.
(45) Guilhabert, B.; Hurtado, A.; Jevtics, D.; Gao, Q.; Tan, H. H.; Jagadish, C.; Dawson, M. D. Transfer Printing of Semiconductor Nanowires with Lasing Emission for Controllable Nanophotonic Device Fabrication. *ACS Nano* **2016**, *10* (4), 3951−3958.
(46) Kim, Y.-H.; Kwon, S.-H.; Lee, J. M.; Hwang, M.-S.; Kang, J.-H.; Park, W. I.; Park, H.-G. Graphene-contact electrically driven microdisk lasers. *Nat. Commun.* **2012**, *3* (1), 1−6.
(47) Daleiden, J.; Eisele, K.; Keller, R.; Vollrath, G.; Fiedler, F.; Ralston, J. D. InGaAsP/InP 1.55-μm lasers with chemically assisted ion beam-etched facets. *Opt. Quantum Electron.* **1996**, *28* (5), 527−532.
(48) Kim, K. S.; Zhao, Y.; Jang, H.; Lee, S. Y.; Kim, J. M.; Kim, K. S.; Ahn, J.-H.; Kim, P.; Choi, J.-Y.; Hong, B. H. Large-scale pattern growth of graphene films for stretchable transparent electrodes. *Nature* **2009**, *457* (7230), 706−710.
(49) Nair, R. R.; Blake, P.; Grigorenko, A. N.; Novoselov, K. S.; Booth, T. J.; Stauber, T.; Peres, N. M. R.; Geim, A. K. Fine Structure Constant Defines Visual Transparency of Graphene. *Science* **2008**, *320* (5881), 1308.
(50) Park, H. J.; Meyer, J.; Roth, S.; Skákalová, V. Growth and properties of few-layer graphene prepared by chemical vapor deposition. *Carbon* **2010**, *48* (4), 1088−1094.
(51) Kim, J.-H.; Aghaeimeibodi, S.; Richardson, C. J. K.; Leavitt, R. P.; Englund, D.; Waks, E. Hybrid Integration of Solid-State Quantum Emitters on a Silicon Photonic Chip. *Nano Lett.* **2017**, *17* (12), 7394−7400.
(52) Choo, H.; Kim, M.-K.; Staffaroni, M.; Seok, T. J.; Bokor, J.; Cabrini, S.; Schuck, P. J.; Wu, M. C.; Yablonovitch, E. Nanofocusing in a metal-insulator-metal gap plasmon waveguide with a three-dimensional linear taper. *Nat. Photonics* **2012**, *6* (12), 838−844.
(53) Falk, A. L.; Koppens, F. H. L.; Yu, C. L.; Kang, K.; de Leon Snapp, N.; Akimov, A. V.; Jo, M.-H.; Lukin, M. D.; Park, H. Near-field electrical detection of optical plasmons and single-plasmon sources. *Nat. Phys.* **2009**, *5* (7), 475−479.
(54) Park, H.; Kuo, Y. H.; Fang, A. W.; Jones, R.; Cohen, O.; Paniccia, M. J.; Bowers, J. E. A hybrid AlGaInAs-silicon evanescent preamplifier and photodetector. *Opt. Express* **2007**, *15* (21), 13539−13546.
(55) Van Campenhout, J.; Rojo Romeo, P.; Regreny, P.; Seassal, C.; Van Thourhout, D.; Verstuyft, S.; Di Cioccio, L.; Fedeli, J. M.; Lagahe, C.; Baets, R. Electrically pumped InP-based microdisk lasers integrated with a nanophotonic silicon-on-insulator waveguide circuit. *Opt. Express* **2007**, *15* (11), 6744−6749.
(56) Xu, Q.; Schmidt, B.; Pradhan, S.; Lipson, M. Micrometre-scale silicon electro-optic modulator. *Nature* **2005**, *435* (7040), 325−327.
(57) Justice, J.; Bower, C.; Meitl, M.; Mooney, M. B.; Gubbins, M. A.; Corbett, B. Wafer-scale integration of group III−V lasers on silicon using transfer printing of epitaxial layers. *Nat. Photonics* **2012**, *6* (9), 610−614.
(58) Liu, L.; Kumar, R.; Huybrechts, K.; Spuesens, T.; Roelkens, G.; Geluk, E.-J.; de Vries, T.; Regreny, P.; Van Thourhout, D.; Baets, R.; Morthier, G. An ultra-small, low-power, all-optical flip-flop memory on a silicon chip. *Nat. Photonics* **2010**, *4* (3), 182−187.
(59) Sun, S.; Zhang, R.; Peng, J.; Narayana, V. K.; Dalir, H.; El-Ghazawi, T.; Sorger, V. J. MO detector (MOD): a dual-function optical modulator-detector for on-chip communication. *Opt. Express* **2018**, *26* (7), 8252−8259.
(60) Brubaker, M. D.; Blanchard, P. T.; Schlager, J. B.; Sanders, A. W.; Roshko, A.; Duff, S. M.; Gray, J. M.; Bright, V. M.; Sanford, N. A.; Bertness, K. A. On-chip optical interconnects made with gallium nitride nanowires. *Nano Lett.* **2013**, *13* (2), 374−377.

https://doi.org/10.1021/acs.nanolett.1c04622
Nano Lett. 2022, 22, 1316−1323